Renewable Energy 175 (2021) 638–649

Contents lists available at ScienceDirect

Renewable Energy

journal homepage: www.elsevier.com/locate/renene

Dynamic modeling and analysis of an advanced adsorption-based osmotic heat engines to harvest solar energy

Yanan Zhao, Mingliang Li, Rui Long*, Zhichun Liu, Wei Liu

School of Energy and power Pngineering, Huazhong University of Science and Technology, Wuhan, 430074, PR China

ARTICLE INFO

Article history:
Received 24 November 2020
Received in revised form
10 April 2021
Accepted 3 May 2021
Available online 12 May 2021

Keywords:
Osmotic heat engines
Solar energy
Reverse electrodialysis
Adsorption
Practical simulation

ABSTRACT

Osmotic heat engine (OHE) is a promising technology to harvest low-grade heat from renewable energy source. In previous studies of OHEs, the features of actual heat source and application scenarios are usually ignored. Here we present an advanced adsorption-based osmotic heat engine to harvest solar energy and a dynamic model for such energy utilization system is established. Firstly, the dynamic characteristics of the OHE from transient to cyclic-steady state is investigated. There exist an optimal adsorption/desorption time to maximize the electric power and efficiency simultaneously. Higher working concentration elevates the electric power and efficiency. Larger direct solar irradiation intensity upgrades the electric power while hinders the efficiency. Then a practical simulation of a small sized OHE harvesting solar energy to generate electricity during a day is carried out and the effects of some important parameters on the system under transient state are analyzed. The results indicate that there is a best number of cycles the system performs during a day to maximize the average electric power and efficiency. Among the ten selected adsorbents, MIL-101 leads to the largest average electric power of 41.8 W and Zeolite 13X leads to the highest electric efficiency of 1.04% when the number of cycles is set as 60 and 7 mol/kg NaCl is employed as working solution.

1. Introduction

The combustion of over-exploited fossil fuels has led to massive greenhouse gas emissions and global warming [1,2], developing efficient thermal system which can utilize clean and renewable energy is a feasible way to solve the dilemma of environment protection and maintaining rapid development [3,4]. Recently, the environment-friendly closed-loop osmotic heat engines (OHEs), which have no environment risk even if operating with hazardous substances as working fluid, attract increasing attentions [5–7].

The OHEs consist of two main components, one is the thermal separation system, where the salt solution is thermally separated into a concentrated solution and a diluted solution to form a salinity gradient, and the other is the power generation system, which extracts electricity from the mixture of the two solutions with different concentrations produced in the thermal separation system. The most common and well established commercial thermal separation technique is membrane distillation (MD), in which the hydrophobic microporous membrane allows water vapor to pass through under the vapor pressure difference between the two sides of the membrane established by a low-grade heat source, while liquid molecules are prevented by the surface tension of the membrane [8,9]. Guillén-Burrieza et al. [10] reported a solar-powered airgap membrane distillation with total membrane area of 9 m^2 for desalination developed by Singaporean enterprise Keppel Seghers, and a highest specific distillation production of 5.09 L h^{-1} m^{-2} and a lowest heat consumption of 294 kWh m^{-3} were obtained. As an emerging desalination technology, adsorption-based desalination (AD) has become a competitive choice for thermal separation components of osmotic heat engine with the advantages of low operating temperature, low energy consumption and process simplicity [11,12]. In AD process, the working saline solution is fed into evaporator where water vapor is evaporated under the force of highly hydrophilic adsorbent, thus the solution remaining in the evaporator is concentrated. The evaporated vapor is adsorbed in the pores of adsorbent then desorbed by heating in the desorption process and finally condensed in

Abbreviations: AD, Adsorption-based desalination; AEM, Anion exchange membrane; CEM, Cation exchange membrane; MD, Membrane distillation; OHE, Osmotic heat engines; PRO, Pressure retarded osmosis; RED, Reverse electrodialysis.

* Corresponding author.
E-mail address: r_long@hust.edu.cn (R. Long).

https://doi.org/10.1016/j.renene.2021.05.010
0960-1481/

Nomenclature

A	Area m^2
A_{ap}	Area of aperture m^2
A_r	Area of receiver m^2
Col_r	Number of modules in series
Col_s	number of the collector rows
c_p	Specific heat capacity J kg^{-1} K^{-1}
D_{so}	A kinetic constant for the silica gel water system m^2 s^{-1}
E	Characteristic energy kJ mol^{-1}
E_a	Activation energy of surface diffusion kJ mol^{-1}
E_{cell}	Electromotive force of one cell V
F	Faraday constant C mol^{-1}
F'	Collector efficiency factor
F_R	Heat removal factor
G_b	direct solar irradiation intensity kW/m^2
f	Spacer shadow factor
h_f	Sensible heat kJ kg^{-1}
h_{fg}	Latent heat kJ kg^{-1}
I	Ion strength of a solution mol L^{-1}
J	Salt or water flux mol $s^{-1}m^{-2}$
j	Current density A m^2
K_γ	Incidence angle modifier
L	Length of the membrane m
M	Mass kg
$\dot{m}$	Mass flow rate kg s^{-1}
N	number of cycles per day
n	Surface heterogeneity factor of the adsorption materials
P	Pressure of adsorption/desorption Pa
P_s	Saturation pressure Pa
P_{RED}	Power W
Q	Heat J
$\dot{Q}$	Power W
$\dot{Q}_r$	Energy rate gained from a single collector W
Q_{st}	Isosteric heat of adsorption kJ kg^{-1}
R	Universal gas constant J mol^{-1} K^{-1}
R_a	Area specific resistance Ω m^2
R_p	Average radius of the adsorbent grains m
S	effective heat absorbed by the receiver W m^{-2}
T	Temperature K
t	Time s
U	Heat transfer coefficient W m^{-2} K^{-1}
V	Volume flow rate m^3 s^{-1}
v	Specific volume m^3 kg^{-1}
W	Uptake of the adsorbent kg^{-1}
W_0	Maximum uptake of the adsorbent kg^{-1}
w	Width of the membrane m
X	Concentration mol kg^{-1}
z	Valency of an ion

Greek Symbols

α	Absorbance of the receiver or permselectivity of the ion-selective membrane in RED
γ	Intercept factor and Activity coefficient
δ	Thickness m
η	Efficiency %
Λ	Molar conductivity S m^2 mol^{-1}
ν	Viscosity m^2 s^{-1}
ρ	Density kg m^{-3}
ρ_c	Reflectance of the mirror
τ	Transmittance of the glass cover

Subscripts

abe	Adsorbate
ads	Adsorption
Brine	Concentrated brine
bed	Adsorption/desorption process
Cond	Condenser
CE	Condenser and evaporator
ch	Chilled water
cw	Cooling water
d	distillate
des	desorption
diff	diffusion
Evap,	Evaporator
eva	Evaporation
env	Environment
g	Gas phase
HX	Heat exchanger
HC	High concentration
hw	Hot water
in	Inlet
LC	Low concentration
m	Membrane
mig	Migration
oil	Thermal oil
out	Outlet
s	Salt
sb	Adsorbent
switch	Switching process
w	Cold water

the condenser producing diluted solution [13–15]. Some researches of AD focused on the numerical simulation and operation strategies are conducted. Wang et al. [16] introduced an experimental investigation of a four-bed AD plant, the results revealed that the optimal switching time is 40s and a maximum specific daily water production of 4.7 kg/kg silica gal was achieved. To improve the performance of the traditional multi-bed AD cycle, Thu et al. [17,18] proposed a re-circulating circuit across evaporator and condenser configuration for internal heat recovery, and twice specific daily water production of conventional AD cycle is obtained. Later, they presented another heat recovery scheme with an evaporator build in the condenser, resulting in triple water production rates. Pressure retarded osmosis (PRO) is commonly employed as a power generation module of OHE, which transport water from diluted solution to concentrated solution driven by salinity gradient with a semipermeable membrane. Then the pressurized concentrated solution is depressurized by a turbine to generate electricity [19,20]. Alternatively, reverse electrodialysis (RED) can also be used to convert salinity gradient energy into electricity. In RED process, a selective permeation of cation/anion through cation exchange membranes (CEMs)/anion exchange membranes (AEMs) along with the electrochemical equilibria at the interface of membranes and solutions leads to the electromotive force in the membrane stack, thus electricity can be obtained by an external load [21–23].

Another attractive advantage of OHE is that it can operate under

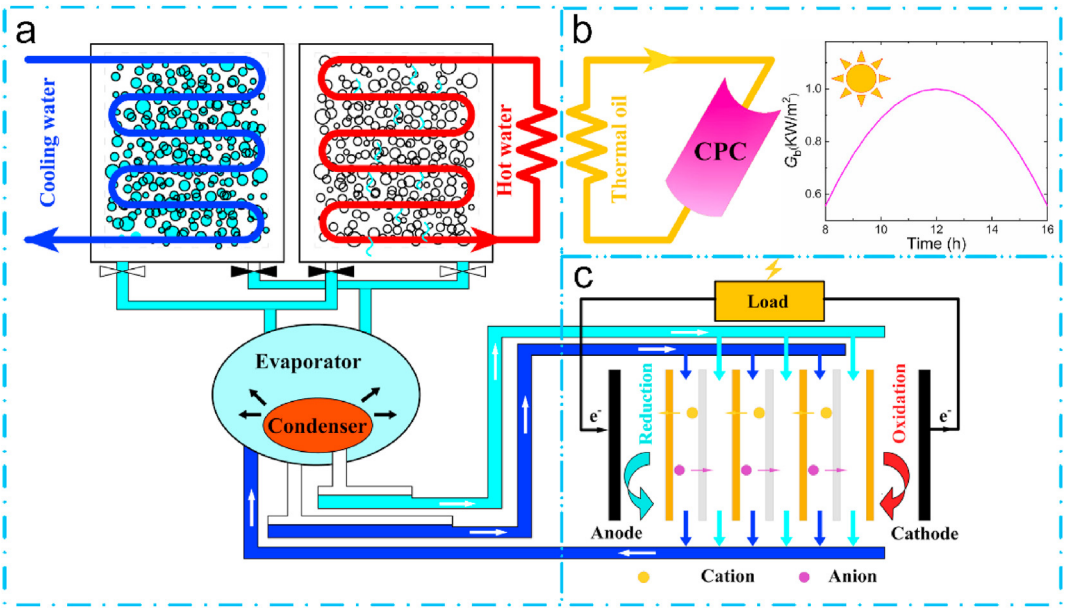

Fig. 1. Schematic diagram of the advanced solar-powered OHE, which consists of a two-bed adsorption-based desalination component with heat recovery scheme for thermal separation (a), a CPC system for harvesting solar energy (b) and a reverse electrodialysis component for electricity generation (c).

heat source below 80 °C [24], which expands the potential application range and fill the gap of utilizing energy from low-grade heat such as industrial waste heat, geothermal energy, solar energy. Solar energy has been wildly investigated due to the advantage of clean, no restriction by geography and large quantity [25,26]. Many different types of OHE configurations for converting low-grade heat into electricity have been proposed. Shaulsky et al. [27] presented a hybrid OHE composed of MD and PRO with methanol as working solvent, and a maximum power density of 72.1 W m^{-2} was achieved when operating under 3 M LiCl-methanol solution. Kwon et al. [28] focused on an OHE system combining RED with ammonium bicarbonate (NH_4HCO_3) solution which is easily decomposed at around 60 °C and an excellent power density of 0.77 W m^{-2} was obtained compared with previous studies. Hickenbottom et al. [29] evaluated different working salt solutions to optimize the performance of the MD-PRO OHE, results indicated that $CaCl_2$ performed well for each performance criteria. Long et al. [30] introduced an MD-RED alternative hybrid OHE, and an electrical efficiency of 1.15% was obtained with 5 mol/kg NaCl as working solution when working at the heat source temperature of 60 °C. Olkis et al. [12] proposed a novel OHE combining RED with AD to harvest low-grade heat, achieving an exergy efficiency of up to 30%. Zhao et al. [31,32] took refrigeration into consideration for the first time and proposed an AD-PRO power and cooling cogeneration system, a maximum exergy efficiency of 33.9% was reported. Long et al. [33] screened MOFs for the AD-PRO heat engines with via molecular simulation and machine learning. A dynamic model of RED-AD cogeneration OHE was further proposed. Hu et al. [34] carried out a theoretical exergy analysis of a MED-RED osmotic heat engine and discussed the effect of structure and operation parameters.

Previous efforts on OHEs mainly highlight the configuration design and optimization, working fluid selection and operating conditions, while the features of heat source and application scenarios are usually ignored. Tong et al. [35] investigated a thermolytic OHE with NH_4HCO_3 as working solution. The feasibility of utilizing the OHE to harvest low-grade heat from industrial waste heat and solar energy was proved. However, the details of the operation process and performance of the OHE under a specific heat source was not further explored. In this study, we present an advanced solar-powered OHE which consists of a two-bed adsorption-based desalination component with heat recovery scheme for thermal separation and a reverse electrodialysis component for electricity generation. The dynamic model is established first, and dynamic responds of the proposed OHE from transient to cyclic-steady state is analyzed. Then a practical simulation of a small sized OHE harvesting solar energy to generate electricity during a day is carried out. The effects of some important operating parameters on system performance under cyclic-steady state and transit state are also discussed.

2. System description and modeling

Fig. 1 shows the schematic diagram of the solar-powered osmotic heat engine, which consists of three subsystems: compound parabolic collector (CPC) system, adsorption desalination system and reverse electrodialysis. The CPC system harvests solar energy and heats the thermal oil to high temperature, then the thermal oil transfers the collected heat to the hot water circuit of AD system. The AD system contains three main components of evaporator, condenser and physical beds. In the AD process, saline solution is fed into the evaporator where the solvent evaporates and the remaining solution is consequently concentrated. The water vapor is then continuously adsorbed by the adsorption bed until the bed is saturated, while cooling water circulates through the bed to remove the adsorption heat. Then the cooling water is switched to hot water which adsorbs heat from CPC, and the vapor is desorbed and condensed in the condenser, thus diluted solution is produced. There is always a switching time between adsorption and desorption for precooling/preheating the adsorption bed and two beds mode enables a semi-continuous operation. A configuration of evaporator incorporating a condenser inside it is construct to recover the latent heat of condensation and the cooling capacity released in evaporation. In the RED process, the concentrated and diluted solutions produced in AD system are supplied alternatively into the cell where IEMs and AEMs are alternatively changed, the cations and anions move in opposite directions driven by the

salinity gradient, thus establishing a potential difference between the electrodes. Finally, the redox reaction on the electrodes converts ionic current into electric current and extracted by an external load. The effluents are recharged into the evaporator of AD to restore the initial concentration.

To simplify the mathematical model, the following assumptions are considered: (1) The pressure, temperature and working capacity of the entire adsorption beds are uniform. The working capacity, temperature and pressure distributions can affect the heat and mass transfer in a real AD system, and a computational fluid dynamic (CFD) model of AD system considering the temperature and pressure distributions was established in our previous study [36,37]. In order to save computing resources, the effects are neglected in this study. (2) Thermal resistance between the adsorbent and the metal tube is neglected. The thermal resistance would weaken the heat transfer between the external hot/cold water and the adsorption bed. (3) Heat loss and flow resistance of the AD system are neglected. Thus, all the components are considered to be adiabatic and pump consumption of the AD system can be ignored. (4) The variation of direct solar irradiation intensity during a day obeys a parabolic relationship, which is a simplified model of solar radiation intensity.

2.1. The CPC system model

The useful energy rate gained from a single solar collector is

$$\dot{Q}_{\mathrm{r}} = \dot{m}_{\mathrm{oil}} c_{p,\mathrm{oil}} (T_2 - T_1) \tag{1}$$

where c_p is the specific heat and $\dot{m}_{\mathrm{oil}}$ is the mass flow rate of the thermal oil. T_1 and T_2 are the temperature at the inlet and outlet of the receiver. The collected energy rate can also be given by Ref. [38].

$$\dot{Q}_{\mathrm{r}} = F_{\mathrm{R}} A_{\mathrm{ap}} \left[S - \frac{A_{\mathrm{r}}}{A_{\mathrm{ap}}} U_{\mathrm{L}} (T_2 - T_0) \right] \tag{2}$$

where F_R is the heat removal factor, A_{ap} and A_{r} is the area of aperture and receiver, U_{L} is the collector overall heat loss coefficient and S is the effective heat absorbed by the receiver, which can be defined as

$$S = G_b \tau \rho_c \alpha \gamma K_\gamma \tag{3}$$

where G_b is the direct solar irradiation intensity, which obeys the parabolic relationship of $G_{\mathrm{b}} = -3 + 0.66667t - 0.02778t^2 (8 \le t \le 16$o'clock), ρ_c, γ, τ, α and K_γ are the reflectance of the mirror, intercept factor, transmittance of the glass cover, absorbance of the receiver, and incidence angle modifier, respectively. The heat removal factor is given by

$$F_{\mathrm{R}} = \frac{\dot{m}_{\mathrm{oil}} c_{p,\mathrm{oil}}}{A_{\mathrm{r}} U_{\mathrm{L}}} \left[1 - \exp\left(\frac{-F' U_{\mathrm{L}} A_{\mathrm{r}}}{\dot{m}_{\mathrm{oil}} c_{p,\mathrm{oil}}} \right) \right] \tag{4}$$

where F' is the collector efficiency factor.

The amount of solar energy irradiated on the collector is considered as the heat entering into the system, which can be expressed as

$$\dot{Q}_{\mathrm{solar}} = A_{\mathrm{ap}} F_{\mathrm{R}} S Col_{\mathrm{r}} Col_{\mathrm{s}} \tag{5}$$

where Col_{r} and Col_{s} are the number of modules in series and the number of the collector rows.

2.2. The AD system model

The estimated vapor uptake by the adsorbent at a specific pressure and temperature is given by Dubinin–Astakhov equation [39].

$$W = W_0 \exp\left\{ - \left[\frac{RT}{E} \ln\left(\frac{P_{\mathrm{s}}}{P} \right) \right]^n \right\} \tag{6}$$

where, W_0 is the maximum uptake, P_{s} and P are the equilibrium pressure and adsorption pressure, respectively.

The instantaneous uptake of the adsorption is expressed via the linear driving force equation as [40].

$$\frac{dW}{dt} = \frac{15 D_{\mathrm{so}} e^{-\frac{\mathrm{Ea}}{RT}}}{R_{\mathrm{p}}^2} (W - W_0) \tag{7}$$

where D_{so} is the kinetic constant and R_{p} is the particle radius.

The overall mass balance of the entire AD system is described as

$$\frac{dM_{\mathrm{s,Evap}}}{dt} = \dot{m}_{\mathrm{s,in}} - \dot{m}_{\mathrm{d,Cond}} - \dot{m}_{\mathrm{Brine}} \tag{8}$$

where, $M_{\mathrm{s,Evap}}$is the amount of the working solution in the evaporator, $\dot{m}_{\mathrm{s,in}}$ denotes the mass flow rate of the solution fed into the evaporator, $\dot{m}_{\mathrm{d,Cond}}$is the mass flow rate of the diluted solution discharged from the condenser and $\dot{m}_{\mathrm{Brine}}$is the mass flow rate of the concentrated solution discharged from the evaporator.

The mass and salt balance in evaporator with working solution feed and solvent evaporation in it is given by

$$\frac{dM_{\mathrm{s,Evap}}}{dt} = \dot{m}_{\mathrm{s,in}} - \dot{m}_{\mathrm{Brine}} - \left(\frac{dW_{\mathrm{ads}}}{dt} \right) M_{\mathrm{sb}} \tag{9}$$

$$M_{\mathrm{s,Evap}} \frac{dX_{\mathrm{s,Evap}}}{dt} = X_{\mathrm{s,in}} \dot{m}_{\mathrm{s,in}} - X_{\mathrm{s,Evap}} \dot{m}_{\mathrm{Brine}} - X_{\mathrm{D}} \left(\frac{dW_{\mathrm{ads}}}{dt} \right) M_{\mathrm{sb}} \tag{10}$$

where $X_{\mathrm{s,Evap}}$, $X_{\mathrm{s,in}}$ and X_{D} are denote the concentration of solution remaining in evaporator, working concentration and the concentration of vapor, respectively.

The energy balance for evaporator which is coupled inside the condenser is written as

$$\begin{aligned} &\left[M_{\mathrm{s,Evap}} c_{\mathrm{p,s}} (T_{\mathrm{Evap}}, X_{\mathrm{s,Evap}}) + M_{\mathrm{HX,Evap}} c_{\mathrm{p,HX}} \right] \frac{dT_{\mathrm{Evap}}}{dt} = h_{\mathrm{f}} (T_{\mathrm{Evap}}, X_{\mathrm{s,Evap}}) \dot{m}_{\mathrm{s,in}} \\ &- h_{\mathrm{fg}} (T_{\mathrm{Evap}}) \frac{dW_{\mathrm{ads}}}{dt} M_{\mathrm{sb}} + U_{\mathrm{CE}} \mathrm{A}_{\mathrm{CE}} (T_{\mathrm{Cond}} - T_{\mathrm{Evap}}) - h_{\mathrm{f}} (T_{\mathrm{Evap}}, X_{\mathrm{s,Evap}}) \dot{m}_{\mathrm{Brine}} \end{aligned} \tag{11}$$

The first and last term on the right side represents the sensible heat of the fed solution and discharged solution, the second term stands for the heat taken away by the vapor evaporated whilst the third represents the heat recovery from the condenser.

The energy balance in condenser is calculated as

$$\left[M_{\mathrm{Cond}}c_{\mathrm{p}}(T_{\mathrm{Cond}})+M_{\mathrm{HX,Cond}}c_{\mathrm{p,HX}}\right]\frac{dT_{\mathrm{Cond}}}{dt}=h_{\mathrm{f}}(T_{\mathrm{Cond}})\frac{dM_{\mathrm{d}}}{dt}+h_{\mathrm{fg}}(T_{\mathrm{Cond}})\frac{dW_{\mathrm{des}}}{dt}M_{\mathrm{sb}}-U_{\mathrm{CE}}\mathrm{A}(T_{\mathrm{Cond}}-T_{\mathrm{Evap}}) \tag{12}$$

The outlet temperature from each heat exchanger is calculated via the log mean temperature difference as

$$T_{\mathrm{out}}=T_0+(T_{\mathrm{in}}-T_0)\exp\left(\frac{-UA}{\dot{m}c_{\mathrm{p}}(T_0)}\right) \tag{13}$$

The energy balance for adsorption/desorption bed with cooling/hot water flowing through is given by

$$\left[M_{\mathrm{sb}}c_{\mathrm{p,sb}}+M_{\mathrm{HX}}c_{\mathrm{p,HX}}+M_{\mathrm{abe}}c_{\mathrm{p,a}}\right]\frac{dT_{\mathrm{ads/des}}}{dt}=\pm Q_{\mathrm{st}}M_{\mathrm{sb}}\frac{dW_{\mathrm{ads/des}}}{dt}\pm\dot{m}_{\mathrm{cw/hw}}c_{\mathrm{p}}\left(T_{\mathrm{cw/hw}}\right)\left(T_{\mathrm{cw/hw,in}}-T_{\mathrm{cw/hw,out}}\right) \tag{14}$$

where Q_{st} denoting the isosteric heat is given by

$$Q_{\mathrm{st}}=h_{\mathrm{fg}}+E\left\{-\ln\left(\frac{W}{W_0}\right)^{1/n}\right\}+Tv_{\mathrm{g}}\left(\frac{\partial P}{\partial T}\right)_{\mathrm{g}} \tag{15}$$

The total regeneration heat consumption which is equal to the collected energy in CPC system can be calculated as

$$Q_{\mathrm{reg}}=\int_0^{t_{\mathrm{cycle}}}\dot{m}_{\mathrm{hw}}c_{\mathrm{p,hw}}(T_{\mathrm{hw,in}}-T_{\mathrm{hw,out}})dt \tag{16}$$

where cycle time $t_{\mathrm{cycle}}=t_{\mathrm{bed}}+t_{\mathrm{switch}}$ is composed of a switching time t_{switch} and an adsorption/desorption time t_{bed}.

2.3. The reverse electrodialysis system model

The reverse electrodialysis system model is developed based on a well validated RED model [41], and NaCl is employed as working salt. The electric voltage of a cell pair is written as [23].

$$E_{\mathrm{cell}}(x)=\alpha_{\mathrm{CEM}}\frac{RT}{F}\ln\frac{\gamma_{\mathrm{HC}}^{\mathrm{Na}}(x)X_{\mathrm{HC}}(x)}{\gamma_{\mathrm{LC}}^{\mathrm{Na}}(x)X_{\mathrm{LC}}(x)}+\alpha_{\mathrm{AEM}}\frac{RT}{F}\ln\frac{\gamma_{\mathrm{HC}}^{\mathrm{Cl}}(x)X_{\mathrm{HC}}(x)}{\gamma_{\mathrm{LC}}^{\mathrm{Cl}}(x)X_{\mathrm{LC}}(x)} \tag{17}$$

where α denotes the membranes permselectivity, the subscripts LC and HC represents low concentration and high concentration, γ is the activity of the solution which can be calculate as [42].

$$\gamma(x)=\exp\left[\frac{-0.51z^2\sqrt{I(x)}}{1+(A/305)\sqrt{I(x)}}\right] \tag{18}$$

The area specific cell pair resistance containing four resistances of two solutions, AEM and CEM is given by Refs. [23,42,43].

$$R_{\mathrm{a,cell}}=R_{\mathrm{LC}}(x)+R_{\mathrm{HC}}(x)+R_{\mathrm{AEM}}+R_{\mathrm{CEM}} \tag{19}$$

where $R_{\mathrm{LC}}=f\frac{\delta_{\mathrm{LC}}}{\Lambda_{\mathrm{LC}}X_{\mathrm{LC}}(x)}$ and $R_{\mathrm{HC}}=f\frac{\delta_{\mathrm{HC}}}{\Lambda_{\mathrm{HC}}X_{\mathrm{HC}}(x)}$, Λ is the molar conductivity,δ is the thicknesses of the channel and f stands for the spacer shadow factor.

The current density is calculated according to the Ohm's law as

$$j(x)=\frac{E_{\mathrm{cell}}(x)}{R_{\mathrm{a,cell}}(x)+R_{\mathrm{a,ext}}(x)} \tag{20}$$

where $R_{\mathrm{a,ext}}(x)$ represent the external load.

The total flux across the membrane composed of the migration term which contributes to ionic current and diffusion term which has hindrance effect [42,44].

$$J_{\mathrm{total}}(x)=J_{\mathrm{mig}}(x)+J_{\mathrm{diff}}(x)=\frac{j(x)}{F}+\frac{2D_{\mathrm{salt}}}{\delta_{\mathrm{m}}}[X_{\mathrm{HC}}(x)-X_{\mathrm{LC}}(x)] \tag{21}$$

where D denotes the permeability coefficient.

The water flux is across the membrane is also considered and given by Ref. [45].

$$J_{\mathrm{water}}(x)=-\frac{2D_{\mathrm{water}}}{\delta_{\mathrm{m}}}[X_{\mathrm{HC}}(x)-X_{\mathrm{LC}}(x)]\frac{M_{\mathrm{H_2O}}}{\rho_{\mathrm{H_2O}}} \tag{22}$$

The mass balance is finally described as [42].

$$\frac{dX_{\mathrm{HC}}(x)}{dx}=-\frac{w}{V_{\mathrm{HC}}}J_{\mathrm{total}}(x)-X_{\mathrm{HC}}(x)\frac{wJ_{\mathrm{water}}(x)}{V_{\mathrm{HC}}} \tag{23}$$

$$\frac{dX_{\mathrm{LC}}(x)}{dx}=\frac{w}{V_{\mathrm{LC}}}J_{\mathrm{total}}(x)+X_{\mathrm{LC}}(x)\frac{wJ_{\mathrm{water}}(x)}{V_{\mathrm{LC}}} \tag{24}$$

where w refers to the width of the membrane and V is the volume flow rate of the solution.

The maximum power can be calculated as$P_{\mathrm{d,max}}(x)=\frac{1}{2}j(x)^2R_{\mathrm{a,cell}}(x)$, thus the total maximum power can be given by

$$P_{\mathrm{max}}=w\int_0^L P_{\mathrm{d,max}}(x)dx \tag{25}$$

The pump loss is also taken into consideration, which is calculated as

$$P_{\mathrm{pump}}=\frac{6\nu_{\mathrm{HC}}V_{\mathrm{HC}}^2}{2w\delta_{\mathrm{HC}}^3}+\frac{6\nu_{\mathrm{LC}}V_{\mathrm{LC}}^2}{2w\delta_{\mathrm{LC}}^3} \tag{26}$$

Consequently, the power can be obtained from the OHE is $P_{\mathrm{RED}}=P_{\mathrm{max}}-P_{\mathrm{pump}}$, and the electric efficiency is $\eta_{\mathrm{e}}=P_{\mathrm{RED}}/Q_{\mathrm{reg}}$.

3. Results and discussion

3.1. Dynamic response from transient to cyclic-steady state

To illustrate the operation process of the osmotic heat engine, the dynamic characteristics with 7 mol/kg NaCl solution and SG A++ as adsorbent under a specific working condition is investigated for the first time, where the temperature of the cooling water is set at 293.15 K, which is equal to the ambient temperature, and the adsorption time and switching time are respectively 460 s and 20 s. The direct solar irradiation intensity at 12 o'clock is employed. Fig. 2a shows the temperature-time history of the physical beds, evaporator and condenser, and it is noted that the system reaches cyclic-steady state in 14–15 cycles after the commence of the computation. Each bed undergoes four processes of precooling, adsorption, preheating and desorption in one cycle, and the two-bed operation mode of the adsorption desalination module in the OHE system enables semi-continuous operation, which leads to a periodic variation in temperature. Due to the temperature

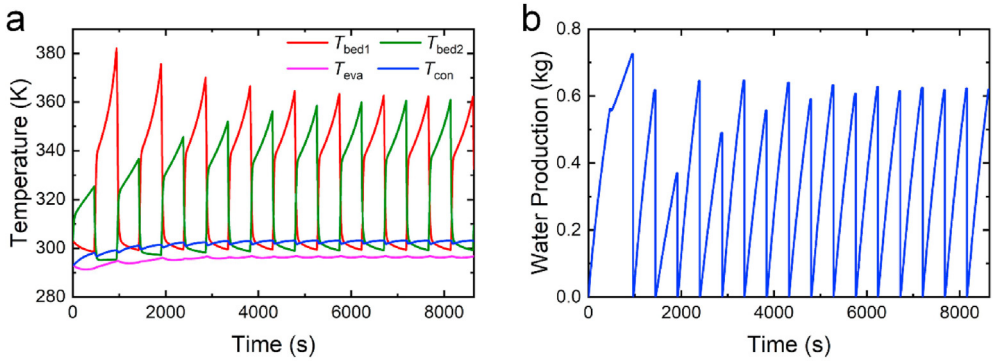

Fig. 2. Temperature profiles of the physical beds, evaporator, condenser (a), and the water production (b) from transient to cyclic-steady state.

difference between evaporator and condenser, the latent heat can be recovered from condenser into the evaporator with the "condenser coupled in evaporator" scheme to facilitate evaporation and condensation. The time variation of water production is given in Fig. 2b, there is always one bed in adsorption process and the other bed in desorption process in a cycle, leading to a periodical water production variation. The water production increases until the end of desorption process and reaches its peak value, then remains constant during switching time. At the end of the cycle, the diluted water produced and the concentrated solution in the evaporator are discharged into the RED module, and the water production returns to zero.

3.2. The effect of operation conditions under cyclic-steady state

As mentioned in previous section, when the system is under cyclic-steady state after 14–15 cycles, state parameters present regular and periodic variation in each cycle. The performance of the solar-powered osmotic heat engine under various operation conditions at cyclic-steady state is investigated. Fig. 3 shows the effects of adsorption/desorption time and working concentration on the performance of the system under the direct solar irradiation intensity of 12 o'clock. The work capacity of the adsorbent denotes the mass of adsorbate adsorbed by 1 kg adsorbent, as seen in Fig. 3b, work capacity of the adsorbent increase with the extension of t_{bed} due to the longer contact time between adsorption bed and water vapor, and the required regeneration heat is positively related to the working capacity, thus Q_{reg} increase as t_{bed}gets longer. Higher concentration lowers the pressure of evaporation, resulting in a reduced work capacity according to the isotherm characteristics of adsorption. There is an optimal adsorption time leading to the maximum electric power as depicted in Fig. 3. At a

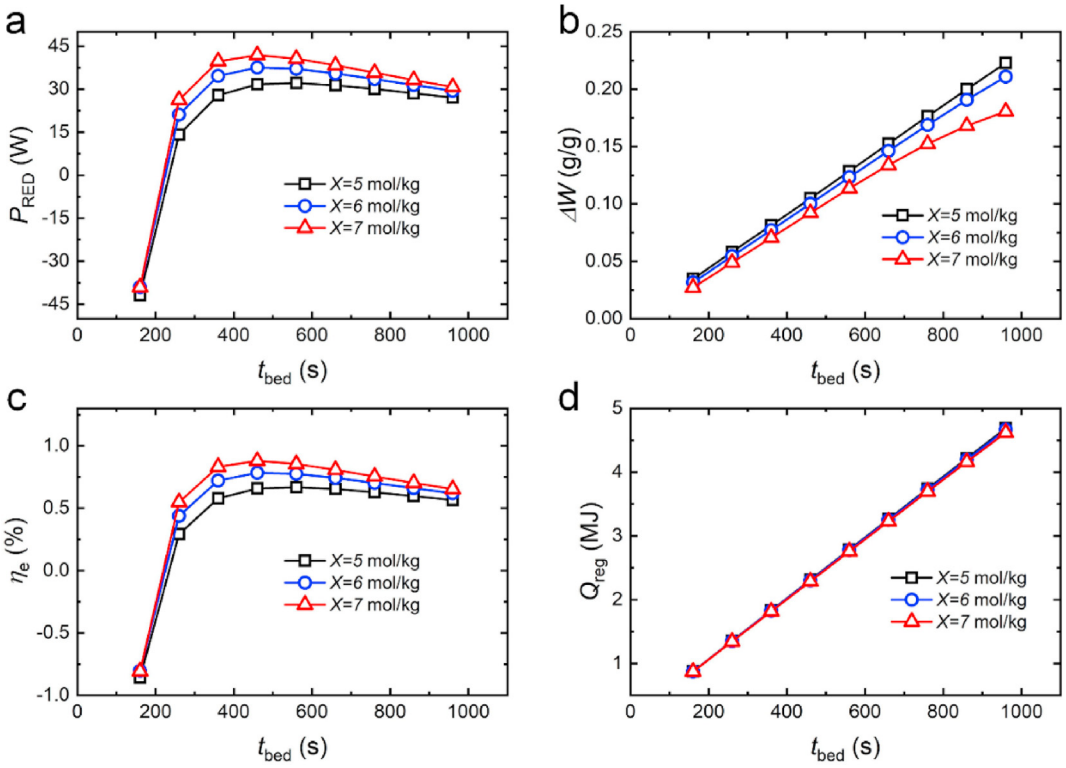

Fig. 3. Electric power (a), work capacity of the adsorbent (b), electric efficiency (c) and Regeneration heat (d) in a cycle under different adsorption/desorption time and working concentration at the direct solar irradiation intensity of 12 o'clock.

shorter t_{bed}, the small work capacity means less work produced in RED, however the pump loss is larger, resulting in negative power. After the electric power reaches its peak value, the increase of work is less than that of cycle period, leading to a reduced power with the extension of t_{bed}. Although high concentration lowers the work capacity, the increased salt gradient in RED overrides the effect, hence the electric power is elevated as concentration increases. At shorter adsorption time, work extracted increases with the increase of t_{bed} due to the elevated working capacity, which contributes to the increase of efficiency. However, the regenerate heat also increases with the increase of t_{bed}, as seen in Fig. 3d, and at longer adsorption time, the increase in the regenerate heat is more significant, which overwhelms the effect of increasing work capacity, thus the electric efficiency decreases. Therefore, there is a maximum value of electric efficiency, and the corresponding t_{bed} is equal to that causes the maximum electric power, as seen in Fig. 3a and d, which indicates that there exist an optimal adsorption/desorption time to maximize the electric power and efficiency simultaneously. A maximum electric efficiency of 0.88% can be obtained. Olkis et al. [46] proposed the application of an AD-RED osmotic heat engine with condensation heat of a steam power plant of 40 °C as energy input, and the maximum energy efficiency can achieve 0.55%.

Fig. 4 demonstrates the effects of the direct solar irradiation intensity on the performance of solar-powered osmotic heat engine, t_{bed} is fixed at 460 s and the direct irradiation intensity of the sun at 17 time points from 8 o'clock to 16 o'clock was selected. The variation of G_b obeys a parabolic relationship with 12 o'clock as axis of symmetry. Larger $G_b$implies more solar energy could be utilized by the CPC system, hence the AD system could have more heat supply for better desorption, resulting in increased working capacity of adsorbent and electric power with increasing G_b, as seen in Fig. 4a and b. However, the electric efficiency decreases as G_b increases, which can be attributed to the more significant increase in heat consumption, as seen in Fig. 4c and d.

3.3. Practical simulation of the solar-powered osmotic heat engine

In practical application scenarios, since the direct solar radiation intensity is constantly changing with time variation, the solar-powered system is always in a transient state. Here, we assume that the direct solar radiation intensity during the two cycles when each adsorption bed undergoes a complete adsorption and desorption process is constant at the average value. NaCl solution with a concentration of 7 kg/mol is employed as working fluid, adsorption time and switching time are set at 460 s and 20 s, respectively. Fig. 5a depicts the temperature variation of the physical beds, evaporator and condenser during a day. It can be seen that the temperature in the four main components of AD system is relatively high at noon due to the highest direct solar radiation intensity at 12 o'clock. However, the maximum temperature does not appear at exactly 12 o'clock but later, since the high temperatures in the components of AD system at the end of one cycle equal to the initial temperature distribution of next cycle, leading to a higher temperature in the next cycle. Then the temperature gradually drops due to the significant decrease in the direct solar radiation intensity. The variation of water production and electric power are both in good agreement with that of temperature, which is due to the better regeneration process at higher temperature. It can also be seen from the Fig. 5b and d that the water production and electric power are different in the two cycles with the same solar radiation intensity due to the different initial operating environment of the two beds in transient state. Fig. 5c shows the accumulated hourly water production, which more intuitively reflects the variation of water production caused by the change of solar radiation intensity during a day.

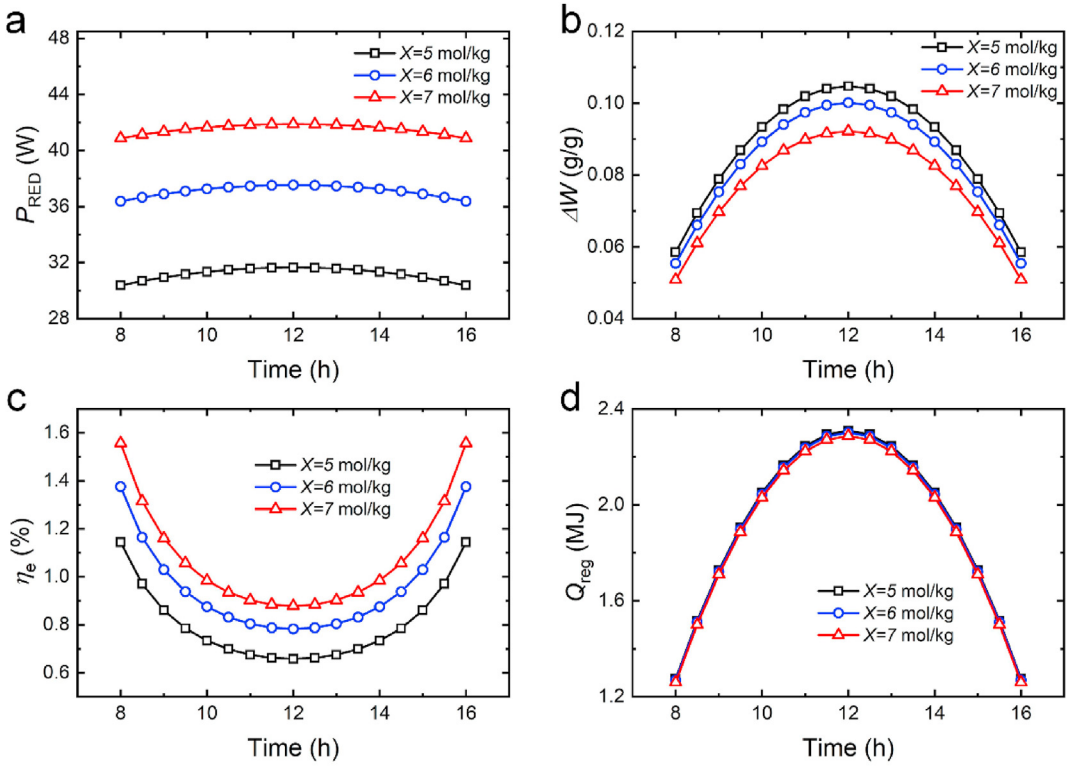

Fig. 4. Electric power (a), work capacity of the adsorbent (b), electric efficiency (c) and Regeneration heat (d) in a cycle under different times of a day and working concentration at $t_{bed}$of 460s.

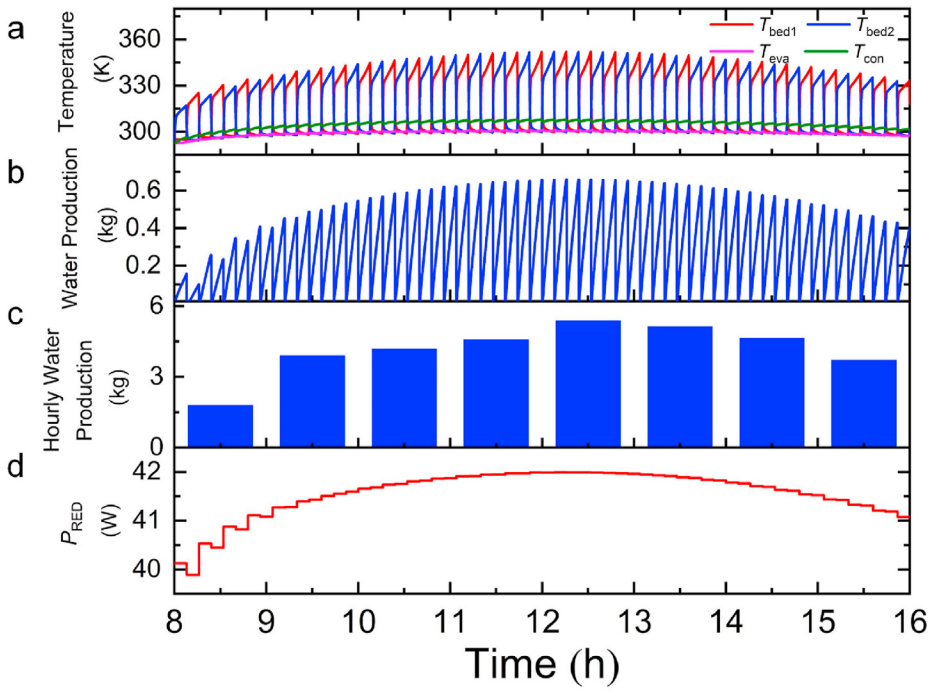

Fig. 5. Temperature profiles of the physical beds, evaporator, condenser (a), the water production (b), the accumulated hourly water production (c) and the electric power (d) during a day.

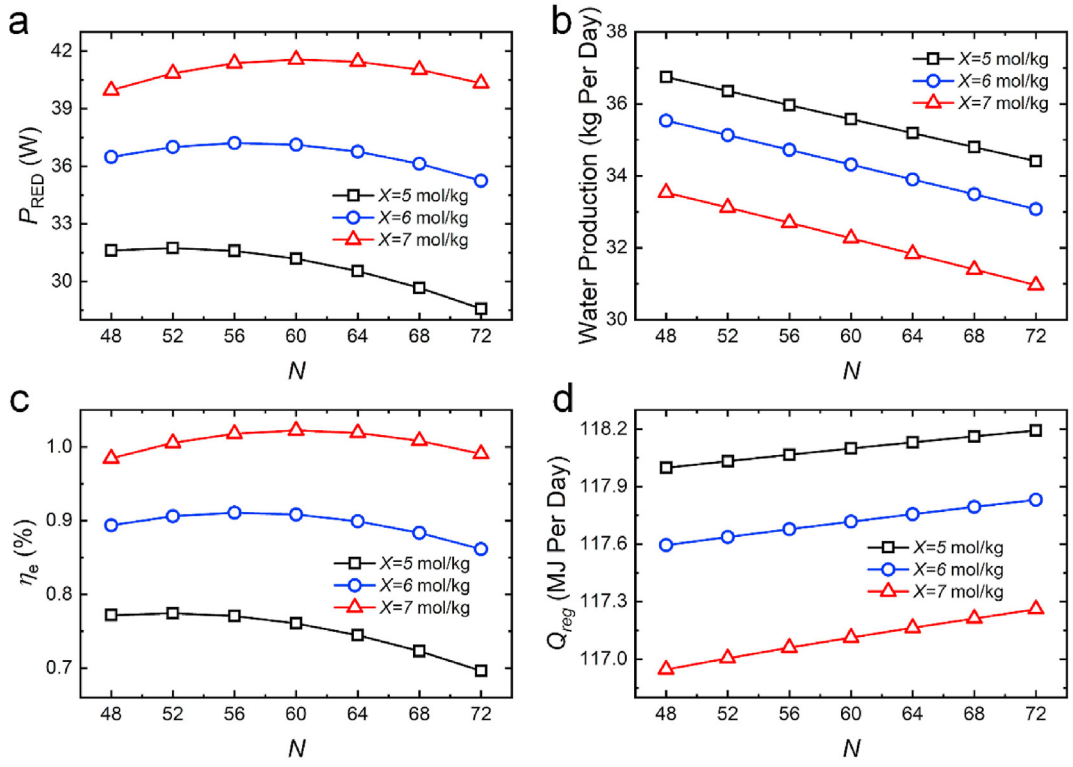

Fig. 6. Average electric power (a), water production (b), electric efficiency (c) and Regeneration heat (d) in a day under different number of cycles and working concentration.

3.4. The effect of operation conditions under transient state

The number of cycles in a day N represents the number of times each physical bed undergoes a complete switching process and adsorption/desorption process in a day (From 8 to 16 o'clock). For example, N = 60 indicates the number of cycles the system performs in a day is 60 and the cycle duration is therefore 480 s. Fig. 6 represents the effect of number of cycles in a day on the performance of the solar-powered system. Switching time is set at 20 s and SG A++ is employed as adsorbent. N can be adjusted by

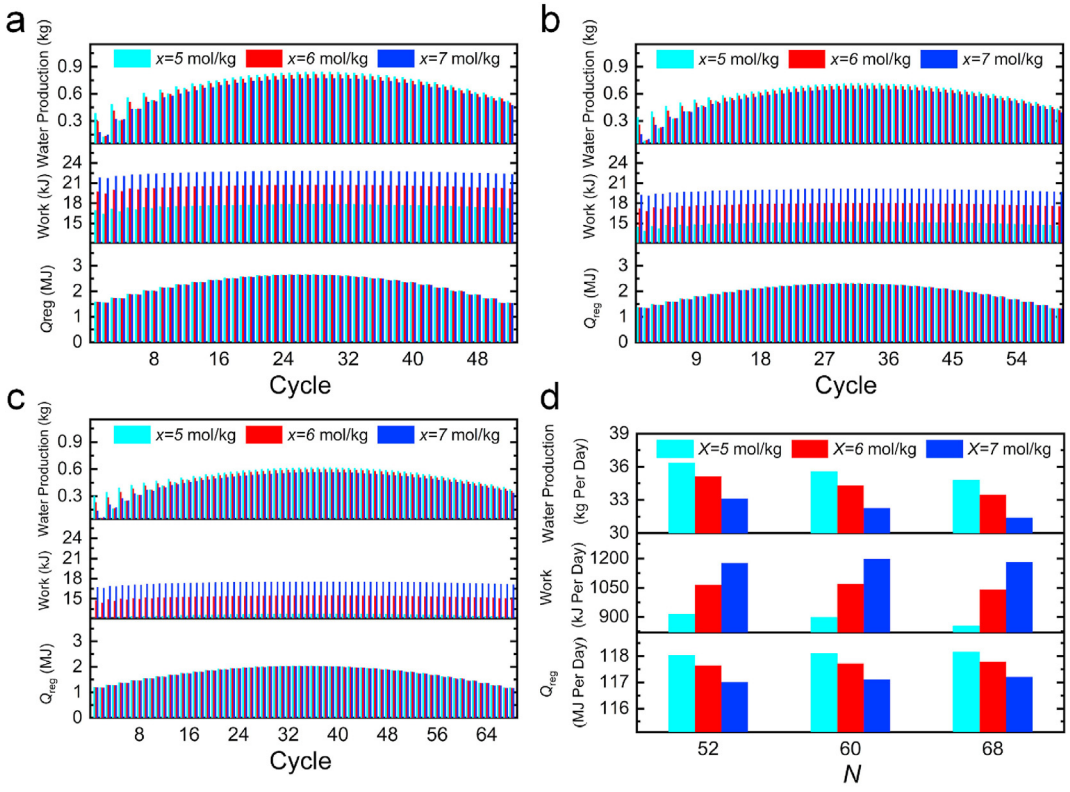

Fig. 7. Water production, work extracted and regeneration heat (a–c) of each cycle during a day and total water production, work extracted and regeneration heat (d) during a day under three different number of cycles and working concentration.

changing the duration of each cycle, which indicates that larger N results in shorter t_{bed}. Fig. 6 shows the variation of average power, average efficiency, total water production and total regenerative heat in a day under different N, while the details of each cycle cannot be reflected. In order to better illustrate the effect of the number of cycles in a day, we further investigated the water production, work extracted and regeneration heat of each cycle during a day in three cases where N is equal to 52, 60, and 68, as seen in Fig. 7. The average electric power first increase with increasing N, reaches its maximum value and then decrease (Fig. 6a). As shown in Fig. 7a–c, larger N leads to less water production of each cycle due to the shorter corresponding t_{bed}, thus the total water production per day is reduced (Fig. 6b). At a larger N, the decrease of water production and increased pump loss both lead to the reduction in work extracted, thereby reducing the average electric power. And at a smaller N, the increase in the number of cycles augments the total work extracted in a day, which overrides the effect of the decreasing work extracted of each cycle. As depicted in Fig. 7d, the total work extracted per day corresponding to N = 60 is higher than that at N = 52 and 68 under the concentration of 7 mol/kg. In addition, with the increase of N, the regeneration heat in each cycle decreases (Fig. 7a–c), which is due to the decrease of water production, however, the total regeneration heat per day increases, as seen in Fig. 6d.

The performance of the solar-powered osmotic heat engine under 10 sorts of adsorbents is depicted in Fig. 8. The number of cycles in a day is set as 60 and 7 mol/kg NaCl is employed as working solution. It can be seen that, adsorbents with higher water production leads to higher average electric power as the result of larger salinity gradient energy generated. The regeneration heat is positively correlated with water production. The efficiency of the adsorbent with higher average electric power is relatively low, however, it is not strictly negative correlation between the power and efficiency due to the different isotherm characteristics of different types of adsorbents. MIL-101 leads to the highest average electric power and Zeolite 13X renders the highest electric efficiency.

We selected the two adsorbents corresponding to the highest average electric power and electric efficiency to compare and analyze their electric power and electric efficiency of each cycle during a day. As seen in Fig. 9, the electric power of each cycle is higher when MIL-101 is employed as adsorbent, however, the electric efficiency of each cycle is low, which can be attributed to the high heat consumption. While the opposite is true when Zeolite 13X is employed as adsorbent.

4. Conclusions

In this study, an advanced solar-powered OHE which consists of a CPC system for harvesting solar energy, a two-bed adsorption-based desalination component with heat recovery scheme for thermal separation and a reverse electrodialysis component for electricity generation is presented and a dynamic model is established. The dynamic characteristics of the OHE from transient to cyclic-steady are discussed. There exist an optimal adsorption/desorption time to maximize the electric power and efficiency simultaneously. Higher working concentration elevates the electric power and efficiency. Larger direct solar irradiation intensity upgrades the electric power while hinders the efficiency. Then a practical simulation of the OHE harvesting solar energy to generate electricity during a day is carried out. Since the system is always at transient state in practical application scenarios, the effects of some important parameters under transient state is also analyzed. There is a best number of cycles the system performs during a day to

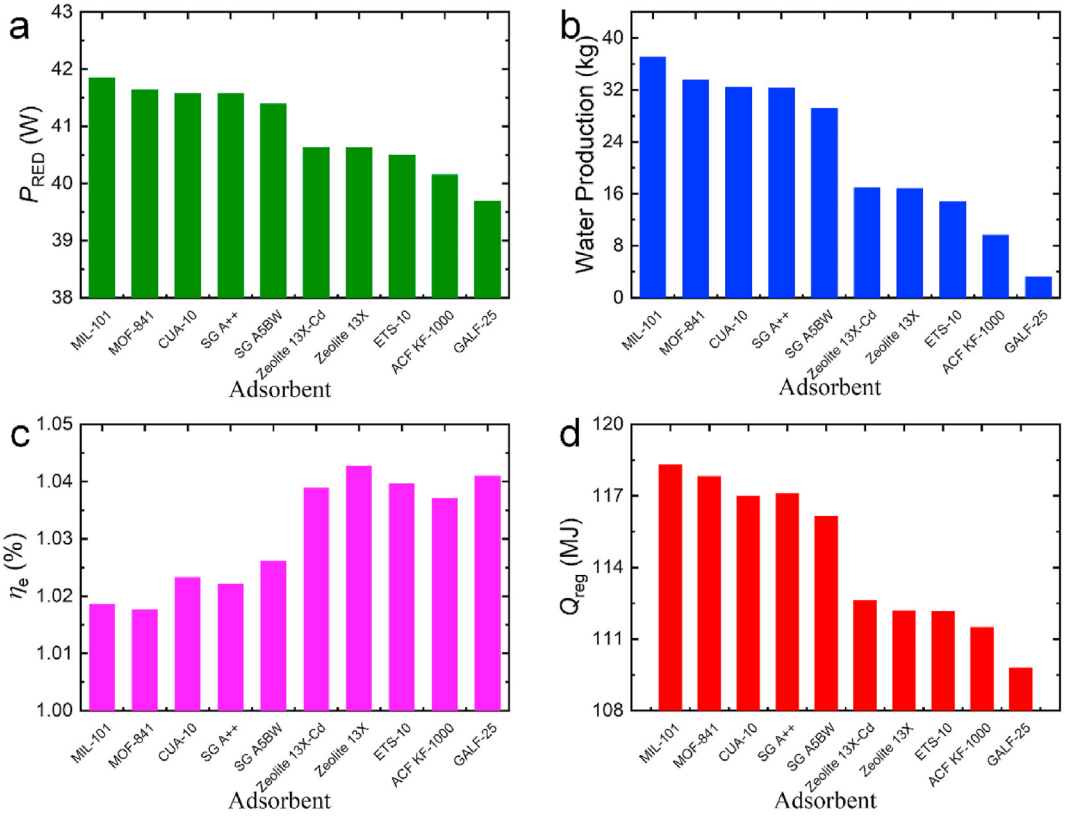

Fig. 8. Average electric power (a), water production (b), electric efficiency (c) and Regeneration heat (d) in a day under different various absorbents.

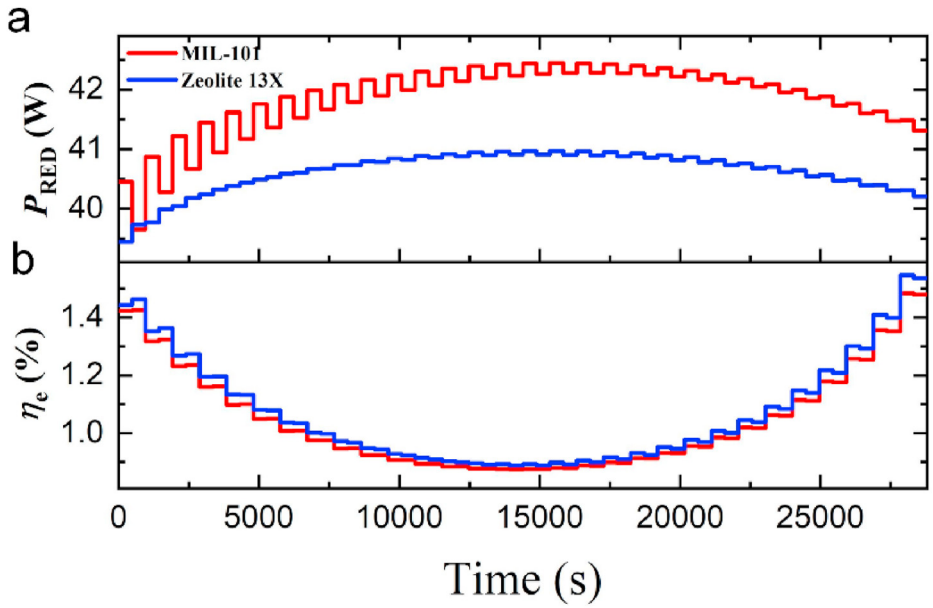

Fig. 9. Electric power (a) and electric efficiency (b) of each cycle during a day with the two adsorbents corresponding to the highest average electric power and efficiency.

maximize the average electric power and efficiency. Among the ten types of adsorbent materials, MIL-101 leads to the largest average electric power of 41.8 W and Zeolite 13X leads to the highest electric efficiency of 1.04% when the number of cycles is set as 60 and 7 mol/kg NaCl is employed as working solution. This study investigates the details of the operation process and the performance of the OHE under a specific heat source of solar energy which demonstrates the feasibility of the osmotic heat engine harvesting solar energy for power generation and the potential practical application.

Declaration of competing interest

The authors declare that they have no known competing

financial interests or personal relationships that could have appeared to influence the work reported in this paper.

Acknowledgements

This work was financially supported by the National Natural Science Foundation of China (51706076, 51736004).

Appendix

A.1. Model validation

In order to validate the present model, a comparison of specific daily water production (SDWP) and specific cooling power (SCP) with experimental data obtained by Alsaman et al. [47] under different hot water temperature ranging from 76.2 to 92.5 °C with silica gal as adsorbent is reported in fig. A1, it can be seen that the results calculated via the present model fit very well with the experimental date of Alsaman et al., indicating the reliability of the present model.

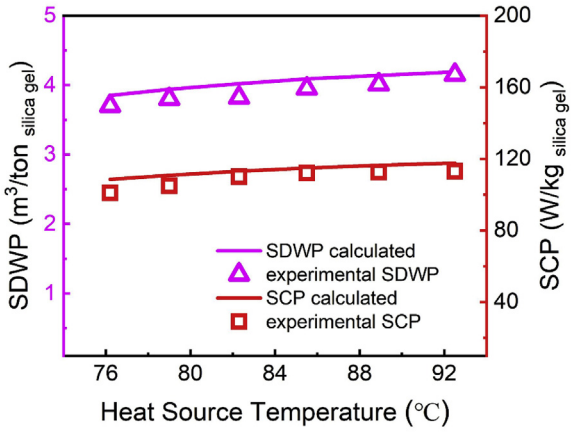

Fig. A1. Comparison of specific daily water production (SDWP) and specific cooling power (SCP) with experimental data obtained by Alsaman et al. under different hot water temperature ranging from 76.2 to 92.5 °C with silica gal as adsorbent.

References

[1] R.E.H. Sims, H.-H. Rogner, K. Gregory, Carbon emission and mitigation cost comparisons between fossil fuel, nuclear and renewable energy resources for electricity generation, Energy Pol. 31 (13) (2003) 1315–1326.
[2] N.L. Panwar, S.C. Kaushik, S. Kothari, Role of renewable energy sources in environmental protection: a review, Renew. Sustain. Energy Rev. 15 (3) (2011) 1513–1524.
[3] R. Long, X. Lai, Z. Liu, W. Liu, Pressure retarded osmosis: operating in a compromise between power density and energy efficiency, Energy 172 (2019) 592–598.
[4] R. Long, Z. Kuang, Z. Liu, W. Liu, Ionic thermal up-diffusion in nanofluidic salinity-gradient energy harvesting, Nat. Sci. Rev. 6 (6) (2019) 1266–1273.
[5] S. Loeb, Method and Apparatus for Generating Power Utilizing Reverse Electrodialysis, US, 1979.
[6] B. Ortega-Delgado, F. Giacalone, P. Catrini, A. Cipollina, A. Piacentino, A. Tamburini, G. Micale, Reverse electrodialysis heat engine with multi-effect distillation: exergy analysis and perspectives, Energy Convers. Manag. 194 (2019) 140–159.
[7] X. Tong, X. Wang, S. Liu, H. Gao, R. Hao, Y. Chen, Low-grade waste heat recovery via an osmotic heat engine by using a freestanding graphene oxide membrane, ACS Omega 3 (11) (2018) 15501–15509.
[8] G. Zaragoza, A. Ruiz-Aguirre, E. Guillén-Burrieza, Efficiency in the use of solar thermal energy of small membrane desalination systems for decentralized water production, Appl. Energy 130 (2014) 491–499.
[9] J. Swaminathan, H.W. Chung, D.M. Warsinger, J.H. Lienhard V, Membrane distillation model based on heat exchanger theory and configuration comparison, Appl. Energy 184 (2016) 491–505.
[10] E. Guillén-Burrieza, G. Zaragoza, S. Miralles-Cuevas, J. Blanco, Experimental evaluation of two pilot-scale membrane distillation modules used for solar desalination, J. Membr. Sci. 409–410 (2012) 264–275.
[11] C. Olkis, S. Brandani, G. Santori, A small-scale adsorption desalinator, Energy Procedia 158 (2019) 1425–1430.
[12] C. Olkis, G. Santori, S. Brandani, An Adsorption Reverse Electrodialysis system for the generation of electricity from low-grade heat, Appl. Energy 231 (2018) 222–234.
[13] P.G. Youssef, H. Dakkama, S.M. Mahmoud, R.K. Al-Dadah, Experimental investigation of adsorption water desalination/cooling system using CPO-27Ni MOF, Desalination 404 (2017) 192–199.
[14] A. Naeimi, S.M. Nowee, H.A. Akhlaghi Amiri, Numerical simulation and theoretical investigation of a multi-cycle dual-evaporator adsorption desalination and cooling system, Chem. Eng. Res. Des. 156 (2020) 402–413.
[15] H.J. Dakkama, P.G. Youssef, R.K. Al-Dadah, S. Mahmoud, Adsorption ice making and water desalination system using metal organic frameworks/water pair, Energy Convers. Manag. 142 (2017) 53–61.
[16] X. Wang, K.C. Ng, Experimental investigation of an adsorption desalination plant using low-temperature waste heat, Appl. Therm. Eng. 25 (17) (2005) 2780–2789.
[17] K. Thu, B.B. Saha, A. Chakraborty, W.G. Chun, K.C. Ng, Study on an advanced adsorption desalination cycle with evaporator–condenser heat recovery circuit, Int. J. Heat Mass Tran. 54 (1) (2011) 43–51.
[18] K. Thu, A. Chakraborty, Y.-D. Kim, A. Myat, B.B. Saha, K.C. Ng, Numerical simulation and performance investigation of an advanced adsorption desalination cycle, Desalination 308 (2013) 209–218.
[19] S. Loeb, Osmotic power plants, Science 189 (4203) (1975) 654.
[20] A. Altaee, G.J. Millar, G. Zaragoza, Integration and optimization of pressure retarded osmosis with reverse osmosis for power generation and high efficiency desalination, Energy 103 (2016) 110–118.
[21] R.A. Tufa, S. Pawlowski, J. Veerman, K. Bouzek, E. Fontananova, G. di Profio, S. Velizarov, J. Goulão Crespo, K. Nijmeijer, E. Curcio, Progress and prospects in reverse electrodialysis for salinity gradient energy conversion and storage, Appl. Energy 225 (2018) 290–331.
[22] B. Ortega-Delgado, F. Giacalone, A. Cipollina, M. Papapetrou, G. Kosmadakis, A. Tamburini, G. Micale, Boosting the performance of a reverse electrodialysis – multi-effect distillation heat engine by novel solutions and operating conditions, Appl. Energy 253 (2019) 113489.
[23] J. Veerman, J. Post, M. Saakes, S. Metz, G. Harmsen, Reducing power losses caused by ionic shortcut currents in reverse electrodialysis stacks by a validated model, J. Membr. Sci. 310 (1–2) (2008) 418–430.
[24] B.E. Logan, M. Elimelech, Membrane-based processes for sustainable power generation using water, Nature 488 (7411) (2012) 313–319.
[25] N.S. Lewis, D.G. Nocera, in: Powering the Planet: Chemical Challenges in Solar Energy Utilization (Proceedings of the National Academy of Science of the United States of America vol. 103, 2006, pp. 15729–15735, https://doi.org/10.1073/pnas.0603395103. Mrs Bulletin 32(10) (2015) 808-820.
[26] R. Sekret, M. Turski, Research on an adsorption cooling system supplied by solar energy, Energy Build. 51 (2012) 15–20.
[27] E. Shaulsky, C. Boo, S. Lin, M. Elimelech, Membrane-based osmotic heat engine with organic solvent for enhanced power generation from low-grade heat, Environ. Sci. Technol. 49 (9) (2015) 5820–5827.
[28] K. Kwon, B.H. Park, D.H. Kim, D. Kim, Parametric study of reverse electrodialysis using ammonium bicarbonate solution for low-grade waste heat recovery, Energy Convers. Manag. 103 (2015) 104–110.
[29] K.L. Hickenbottom, J. Vanneste, T.Y. Cath, Assessment of alternative draw solutions for optimized performance of a closed-loop osmotic heat engine, J. Membr. Sci. 504 (2016) 162–175.
[30] R. Long, B. Li, Z. Liu, W. Liu, Hybrid membrane distillation-reverse electrodialysis electricity generation system to harvest low-grade thermal energy, J. Membr. Sci. 525 (2017) 107–115.
[31] Y. Zhao, Z. Luo, R. Long, Z. Liu, W. Liu, Performance evaluations of an adsorption-based power and cooling cogeneration system under different operative conditions and working fluids, Energy 204 (2020) 117993.
[32] Y. Zhao, M. Li, R. Long, Z. Liu, W. Liu, Dynamic modelling and analysis of an adsorption-based power and cooling cogeneration system, Energy Convers. Manag. 222 (2020) 113229.
[33] R. Long, X. Xia, Y. Zhao, S. Li, Z. Liu, W. Liu, Screening metal-organic frameworks for adsorption-driven osmotic heat engines via grand canonical Monte Carlo simulations and machine learning, iScience 24 (1) (2021) 101914.
[34] J. Hu, S. Xu, X. Wu, D. Wu, D. Jin, P. Wang, L. Xu, Q. Leng, Exergy analysis for the multi-effect distillation - reverse electrodialysis heat engine, Desalination 467 (2019) 158–169.
[35] X. Tong, S. Liu, J. Yan, O.A. Broesicke, Y. Chen, J. Crittenden, Thermolytic osmotic heat engine for low-grade heat harvesting: thermodynamic investigation and potential application exploration, Appl. Energy 259 (2020) 114192.
[36] M. Li, Y. Zhao, R. Long, Z. Liu, W. Liu, Computational fluid dynamic study on adsorption-based desalination and cooling systems with stepwise porosity distribution, Desalination 508 (2021) 115048.
[37] M. Li, Y. Zhao, R. Long, Z. Liu, W. Liu, Gradient porosity distribution of adsorbent bed for efficient adsorption cooling, Int. J. Refrig. (2021), https://doi.org/10.1016/j.ijrefrig.2021.03.013. In press.
[38] F.A. Al-Sulaiman, Exergy analysis of parabolic trough solar collectors integrated with combined steam and organic Rankine cycles, Energy Convers. Manag. 77 (2014) 441–449.
[39] A.A. Askalany, M. Salem, I.M. Ismail, A.H.H. Ali, M.G. Morsy, Experimental study on adsorption–desorption characteristics of granular activated carbon/R134a pair, Int. J. Refrig. 35 (3) (2012) 494–498.
[40] B.B. Saha, T.J.A.T. Kashiwagi, Experimental investigation of an advanced

adsorption refrigeration cycle, Build. Eng. 103 (1997) 50.
[41] F. Giacalone, P. Catrini, A. Tamburini, A. Cipollina, A. Piacentino, G. Micale, Exergy analysis of reverse electrodialysis, Energy Convers. Manag. 164 (2018) 588–602.
[42] J. Veerman, M. Saakes, S.J. Metz, G.J. Harmsen, Reverse electrodialysis: a validated process model for design and optimization, Chem. Eng. J. 166 (1) (2011) 256–268.
[43] R. Long, B. Li, Z. Liu, W. Liu, Reverse electrodialysis: modelling and performance analysis based on multi-objective optimization, Energy 151 (2018) 1–10.
[44] R. Long, B. Li, Z. Liu, W. Liu, Performance analysis of reverse electrodialysis stacks: channel geometry and flow rate optimization, Energy 158 (2018) 427–436.
[45] J. Veerman, R.M. de Jong, M. Saakes, S.J. Metz, G.J. Harmsen, Reverse electrodialysis: comparison of six commercial membrane pairs on the thermodynamic efficiency and power density, J. Membr. Sci. 343 (1) (2009) 7–15.
[46] C. Olkis, S. Brandani, G. Santori, Adsorption reverse electrodialysis driven by power plant waste heat to generate electricity and provide cooling, Int. J. Energy Res. 45 (2) (2021) 1971–1987.
[47] A.S. Alsaman, A.A. Askalany, K. Harby, M.S. Ahmed, Performance evaluation of a solar-driven adsorption desalination-cooling system, Energy 128 (2017) 196–207.